- **Associate Editor**

Comment to the author

The authors are suggested to carefully check the current version of the paper. Many typos or unclear expressions need to correct. Furthermore, the dynamic performance is expected to add for the demonstration.

Dear Associate Editor,

The revised version is the result of a complete edition conducted by an English institute in Tehran. Moreover, new experimental results are presented in the revised version in order to verify the dynamic performance of the system.

- **Reviewer: 1**

Comment to the author

The topic of the paper is certainly interesting and the inclusion of experimental verification is encouraging. However, I have a few concerns with the paper:

(1) The legends of figures should be unified. For example , the legend styles of Figs. 5~8 should be same with those of Figs. 10~12
The legends of all figures of the essay are unified in the revised version.

(2) The PV module parameters in the simulation part differ from those in the experiments. Is it possible to permit the congruence of those parameters so as to make sense of the simulated results?
To prevent ambiguity, in the revised version, simulation results are presented based on the same parameters of the PV panel used for experimental implementation.

(3) It is a pity that dynamic performance of the system is not verified in the experiment. It is recommended that experiments about dynamic performance such as the step changes in irradiance, as indicated in simulation, should be carried out in the Section 6.
New experimental results are presented in the revised version (Fig. 12) in order to verify the dynamic performance of the system.

(4) Overall, the use of English should be improved.
The revised version is the result of a complete edition conducted by an English institute in Tehran.

- **Reviewer: 2**

Comment to the author

This paper proposes a two-switch flyback inverter for fractional horse power water pumping systems, which can mitigate the high-voltage transients at turn-off switching state and integrate the sensorless MPPT and constant v/f control. The proposed scheme exhibits salient advantages by comparing with single flyback inverters and achieves the efficient utilization of both PV panels and electric motors.

(1) In the Abstract, the first word is incorrect, which should be flyback.
It is corrected at the revised version.

(2) The author needs to give the full name of MPPT in the abstract.
It is corrected at the revised version.

(3) The word "Where" followed by equations should be in lowercase rather.
It is corrected at the revised version.
(4) In references, the abbreviation of Journals should be in accordance with the standard.
The references are edited in accordance with the IET's journal standard.
(5) The font of figures is too small, which is difficult for readers. So authors are suggested to adjust the font size.
The font size of figures is adjusted at the revised version.
(6) In figure 8, the irradiance is halved twice. The author is suggested to add an additional case study where the irradiance is increased.
Both decreasing and increasing scenarios are presented in the revised version (Fig. 6).
(7) The writing should be further polished. The current version is not qualified for IET journals.
The revised version is the result of a complete edition conducted by an English institute in Tehran.

A two-switch flyback inverter employing a current sensorless MPPT and scalar control for low cost solar powered pumps

F. Karbakhsh [a], Mehdi Amiri [b], H. Abootorabi Zarchi [a*]

[a] Electrical Engineering Department, Faculty of Engineering, Ferdowsi University of Mashhad, Mashhad, Iran

[b] School of Electrical and Computer Engineering, University of Tehran, Tehran, Iran

*abootorabi@um.ac.ir

***Abstract*—** Flyback inverter is known as a low cost solution for photovoltaic ac module application. This paper presents a two-switch flyback inverter followed by a low frequency unfolding bridge for fractional horse power water pumping systems. This topology mitigates the problem of high-voltage transients at switch turn off which commonly exists in single switch flyback inverters. Moreover, the proposed control strategy achieves an integration of a novel sensorless maximum power point tracking algorithm as well as a constant *v/f* control for the efficient utilization of both the photovoltaic panel and the motor. The proposed control algorithm minimizes the cost and simplifies the control strategy. The validity and capability of the proposed method are verified by both simulation and practical results of a DSP-based two-switch flyback solar micro inverter for a fractional horsepower water pumping system.

1. INTRODUCTION

In distributed low-power electrical generation applications, photovoltaic (PV) technology is of great importance. Modularity and incessant reduction of price per peak watt over recent years are some of its tempting characteristics. Water pumping is one of the most encouraging applications of off-grid photovoltaic systems. Since lead-acid batteries are heavy, expensive, and have shorter lifetime compared to photovoltaic panels, in photovoltaic applications, it is favorable to use pump-storage systems instead which store solar energy as the potential energy in water reservoir to be consumed according to the demand [1].

In some cases, PV-powered water pumps are based on the usage of DC motors either directly coupled or via DC-DC converter [2]. The need for continuous maintenance and high cost of DC motors restricts the application of DC motors in water pumping systems. A low cost, low maintenance, and reliable solution for PV powered water pumping systems is satisfied by induction motors (IM). Particularly, in household applications, the available ac motors are single phase ones.

In variable frequency drive applications, scalar control (*V/f* control) is typically employed as a speed control technique. The control mechanism feeds the motor with variable frequency Pulse Width Modulation (PWM) signals generated by a full bridge inverter circuit. To get constant torque over the operating range, the *V/f* ratio has to be kept constant. This control scheme is known as "scalar control", since only magnitudes of the input variables, i.e. frequency and voltage, are controlled [3,4], This can be implemented by an open loop control system.

The PV generator (PVG) exhibits nonlinear I–V and P–V characteristic curves. The maximum power produced depends on both irradiance and temperature; thus, maximum power point tracking (MPPT) control unit is required to run the system at the optimized point.

Many different MPPT algorithms have been proposed in literature [5-17]. Among these, the most widely used ones are "perturb and observe (P&O)" and "hill-climbing" algorithms. While simplicity of implementation and reduced number of measured parameters are merits of these MPPT algorithms, the tradeoff in choosing the increment value, which adjusts the control parameter, is the drawback. To decrease losses in steady state, the mentioned increment value must be small while small values worsen the dynamic behavior in the case of rapid changes in the environmental conditions or load characteristics [7-9]. To overcome this deficiency, the adaptive strep size MPPT algorithms have been proposed; however, these

sophisticated algorithms result in increased computational load which leads to slow dynamic response and needs costly hardware.

Recently, many sensorless MPPT algorithms have been proposed to eliminate PV current and/or voltage sensors [18-21] minimizing the cost. Typically, for the two-stage converter topologies, sensorless MPPT algorithms are based on the measurement of DC bus voltage or converter output current [22-23]. For the single stage converter topology discussed in [24], the PV panel current and DC bus voltage is required for the proposed MPPT algorithm. In [25], besides PV panel voltage, the grid current and voltage are sensed. It is notable that these MPPT techniques require at least one sensing element on the DC side of the converter which needs to be filtered in order to determine the average DC component. This entails more processing.

In this paper, the proposed MPPT method requires only to sense the output voltage of the inverter. With a view to minimizing the cost and complexity of the control scheme, this paper presents a novel MPPT scheme with reduced number of sensors.

To improve the dynamic behavior of the system, an optimized converter for interfacing with the PVG is required. The flyback inverter which is derived from the flyback converter is widely used due to its simple structure, low cost, and high efficiency [26]. In [27], a flyback DC/DC converter with high frequency isolation along with an H-bridge PWM inverter is analyzed as a two-stage approach. As both stages operate at high frequency, total loss is relatively high. In [28-31], the single-stage flyback inverter with center-tapped secondary winding is presented. In [32], an interleaved flyback micro-inverter is presented, and the BCM and DCM control strategies have been investigated.

The main drawback of the conventional flyback inverter is the high voltage and current stresses that suffers the switches. At switch turn-off, high-voltage transients are caused by the resonant behavior of the transformer leakage inductance and the transistor output capacitance, resulting in a high-voltage stress. As the amplitude of parasitic ringing is hard to predict, the designer has to choose a transistor with a high voltage rating that typically has a high on-state resistance which leads to high conduction losses.

A solution to remove ringing in the single-switch flyback converter is to use the two-switch flyback converter. The maximum voltage stress of the switches in a two-switch flyback converter is limited only to the DC input voltage, reducing the switching and conduction losses. In [33], a two-stage flyback micro-inverter has been proposed. Existence of one additional high frequency power conversion stage has a negative effect on the overall converter efficiency.

In this paper, a two-switch flyback inverter followed by a low frequency unfolding bridge is employed for fractional horse power water pumping purposes. The proposed control strategy achieves an integration of a novel sensorless MPPT algorithm as well as a constant *v/f* control for the efficient utilization of both the PV panel and the motor.

This paper is organized as follows. Section 2 presents the analysis of the two-switch flyback inverter. Section 3 presents the parameter design procedure. Section 4 presents the proposed control method and its principle of operation. Section 5 provides the simulation results. Finally, in order to verify the performance of the proposed system, experimental results are presented in Section 6.

2. ANALYSIS OF TWO SWITCH-FLYBACK INVERTER

The proposed topology is shown in Fig. 1. It comprises of a two-switch flyback converter, an unfolding bridge, and a C-L filter. S_{m1} and S_{m2} are the main power switches. D_1 and D_2 are the clamping diodes; D_3 is the rectifier diode. n is the transformer turns ratio. S_1-S_4 form a current-source invrter (CSI) to unfold the rectified sinusoidal waveform to the motor. L_m and L_{l1} are the magnetizing and leakage inductances of the transformer respectively. It should be noted that the system is analyzed under discontinuous conduction mode (DCM).

2.1 Analysis of the proposed two-switch flyback inverter under discontinuios conduction mode

In each switching cycle, there are six different modes of operation. In this study, transistor output capacitances have been neglected, therefore, there would be four operational stages [34]. The principle of operation during each stage is explained using equivalent circuits at different stages of a switching cycle shown in Fig. 2.

First stage ($t_0 \leq t < t_1$): At time $t = t_0$ both main switches S_{m1} and S_{m2} are turned on. Since the clamping diode voltages $V_{D1}=V_{D2}= -V_{in}$, the clamping diodes D_1 and D_2 are reversely biased. Assuming that the leakage inductance is much smaller than the magnetizing one, i.e. $L_l << L_m$, the voltage across the magnetizing inductance is approximately V_{in}. It is worth noting that the switches S_{m1} and S_{m2} turn on softly as the leakage inductance L_l limits the rate of rise of current. The current flowing through switches, the leakage inductance, and the magnetizing inductance is given by (1):

$$i_{Lm} = i_{Ll} = \frac{V_{in}}{L_m+L_l}(t - t_0) + i_{Lm}(t_0) \quad (1)$$

where $i_{Lm}(t_0) = 0$. The magnetizing inductance peak current is given by:

$$i_{Lm}(t_1) = \frac{V_{in}dT_s}{L_m+L_l} \quad (2)$$

During this stage the voltages across the main switches V_{S1} and V_{S2} are zero. This stage ends when both switches are turned off by the gate driver.

Second stage ($t_1 \leq t < t_2$): During this stage, switches S_{m1} and S_{m2} are OFF, the diodes D_1 and D_2 are ON, and D_3 is OFF. The voltage across each switch is clamped to $V_1 + V_F$, where V_F is the forward voltage of clamping diode.

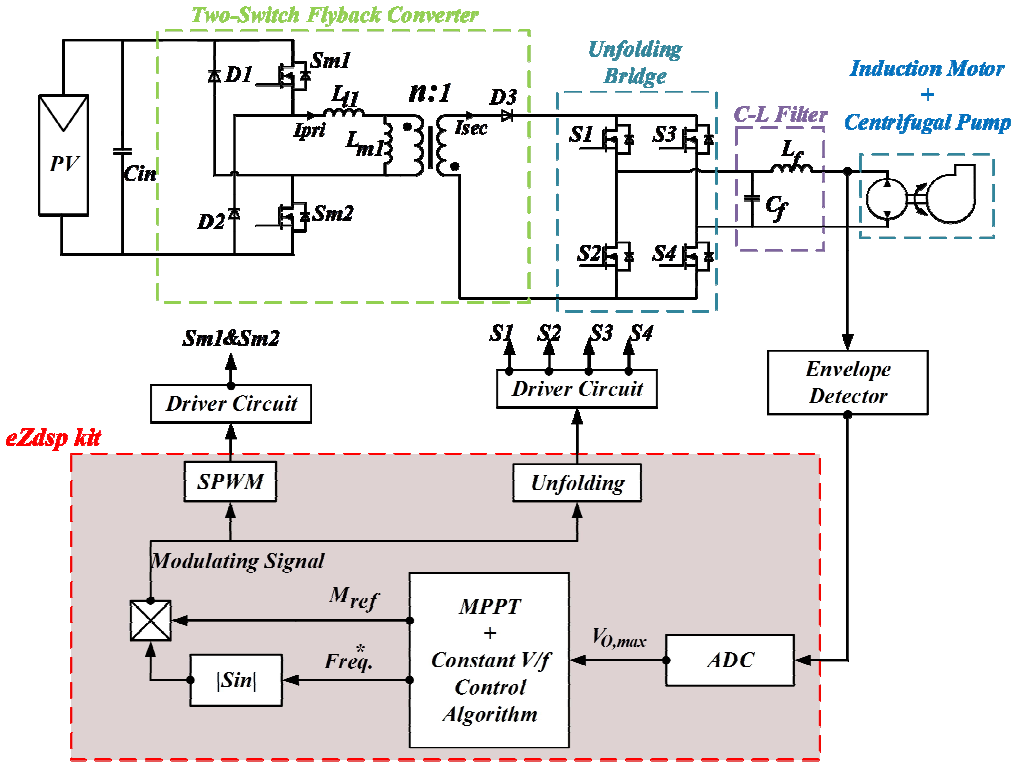

Fig. 1 *The proposed inverter with simultaneous implementation of a current sensorless MPPT and constant v/f control for solar powered pumps*

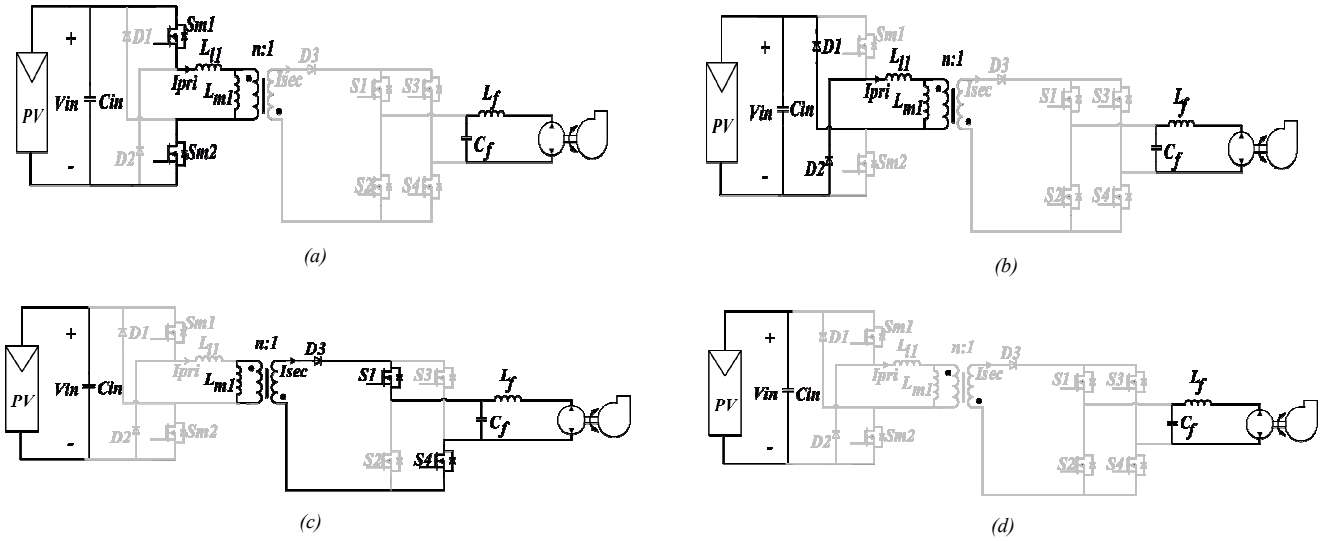

Fig. 2 *Equivalent circuits of the two-switch flyback inverter for DCM at different switching stages. (a) First stage ($t_0 \le t < t_1$). (b) Second stage ($t_1 \le t < t_2$). (c) Third stage ($t_2 \le t < t_3$). (d) Fourth stage ($t_3 \le t < t_4$)*

The current flowing through the magnetizing and leakage inductances which charges the input voltage source V_{in} via clamping diodes D_1 and D_2 is given by (3):

$$i_{Lm} = i_{Ll} = -\frac{V_{in}}{L_m + L_l}(t - t_1) - i_{Lm}(t_1) \tag{3}$$

where $i_{Lm}(t_1)$ is the initial current of the magnetizing inductance at time t_1. This mode is referred to as regenerative clamping mode. This mode comes to an end when the voltage across the magnetizing inductance equals $-nV_O$ thereby forward biasing the rectifier diode D_3.

Third stage ($t_2 \le t < t_3$): At this time interval, switches S_{m1}, S_{m2}, and the clamping diodes are OFF, while the rectifier diode D_3 is ON. The voltage across the magnetizing inductance is:

$$V_{Lm} = -nV_O \tag{4}$$

where V_O is the output voltage. The current flowing through the magnetizing inductance is given by:

$$i_{Lm} = i_{Ll} = -n\frac{V_O}{L_m}(t - t_2) + i_{Lm}(t_2) \tag{5}$$

where $i_{Lm}(t_2)$ is the initial current of the magnetizing inductance at time $t = t_2$, and $n = {N_p}/{N_s}$. N_p and N_s are the number of turns in the primary and secondary windings of transformer respectively.

Assuming that the main switches S_{m1} and S_{m2} are identical, the voltages across switches are:

$$V_{sm1} = V_{sm2} = \frac{V_{in} + nV_O}{2} \tag{6}$$

During this stage, the currents flowing through the main switches, clamping diodes, and the leakage inductance are zero. This stage ends at the time when the rectifier diode current I_{D3} reaches zero.

Fourth stage ($t_3 \leq t < t_4$): In this mode, all the switches and diodes are OFF. The capacitor C_f and the inductor L_f transfer the stored energy to the load. At this time interval, the voltage across switches would be:

$$V_{sm1} = V_{sm2} = \frac{V_{in}}{2} \tag{7}$$

3. DESIGN PROCEDURE

In the case of selecting turns ratio, there is a limitation as follows:

$$n \times V_{O,max} < V_{in} \tag{8}$$

where $V_{O,max}$ is the maximum output voltage, V_{in} is the input voltage, and n is the transformer turns ratio.

To reassure that the micro inverter will always work under DCM, the following limitation should be taken into account [32]:

$$d_{max} \leq \frac{V_{O,max}}{\frac{1}{n}V_{in}+V_{O,max}} \tag{9}$$

where d_{max} is the maximum duty cycle.

The specifications are as follow: input voltage (open circuit voltage): V_{in} =30 V; maximum output voltage $V_{O,max}$=$110\times\sqrt{2}$ V; switching frequency: f_s =40 kHz;

Considering the above specification, turns ratio must be smaller than 0.3. The average primary current is [32]:

$$I_{P,avg} = \frac{1}{4}\frac{V_{in}T_s d_{max}^2}{L_P} \tag{10}$$

where L_p is the transformer primary inductance. The input power is defined as below:

$$P_{pv} = 2V_{in}I_{P,avg} = \frac{1}{2}\frac{V_{in}^2 T_s d_{max}^2}{L_P} \tag{11}$$

Considering P_{PV}=185 W, V_{in}=30 V and d_{max}=0.31, the maximum transformer primary inductance would be $L_{P,max}$=5.84 µH. Therefore, L_P is assumed to be $0.8L_{P,max}$ which equals 4.67 µH.

The input electrolyte capacitor C_{in} is used to compensate the unbalance of constant output power of PV and pulsating power transferred to the load. So, the value of the input capacitor is determined by the energy has to be stored in it, according to [32], the size of this capacitor is:

$$C_{in} = \frac{P_{pv}}{\omega V_{in}\Delta V} \tag{12}$$

where ω is the angle frequency of output voltage, and ΔV is the maximum peak to peak voltage ripple of the input capacitor. To limit the ripple to two volts at the rated output frequency, the required capacitance is:

$$C_{in} \geq 10\ mF \tag{13}$$

The output CL filter shown in Fig. 1 is a second-order low-pass filter with a resonant frequency f_r, which can be expressed as [38]:

$$f_r = \frac{1}{2\pi\sqrt{L_f C_f}} \tag{14}$$

where L_f and C_f are the output filter inductance and capacitance respectively. According to [38], f_r should comply with:

$$10f_0 \leq f_r \leq \frac{1}{10}f_s \tag{15}$$

where f_s is the switching frequency and f_0 is the output rated frequency. Considering (15) and requirements of volume and cost, the values of C_f and L_f must be selected.

4. PRINCIPLES OF THE PROPOSED MPPT AND THE CONTROL ALGORITHM

The purpose of MPPT is to extract the maximum available power from the PV array at any given environmental conditions. When the PV array is connected to a power converter, maximizing the PV array power also maximizes the output power at the output terminals of the converter. Conversely, maximizing the output power of the converter should maximize the PV array power, neglecting the converter losses [35]. It should be noted that most of the practical loads applied in PV systems can be modelled by a voltage source, a resistive, or a combination of both. Therefore, the MPPT can be verified by maximization of either output voltage or current without sensing the second parameter, nor multiplication [36].

In this paper, to achieve MPPT, the envelope of the output voltage $V_{O,max}$ is detected via simple analogue circuit. The voltage is sensed via A/D converter and is compared with the pervious sample. If the new voltage sample is greater than the last one, the MPPT algorithm increases the value of M_{ref}, and vice versa. M_{ref} determines the amplitude of the sinusoidal modulating signal which is used for generating gate drive signals. The flowchart of the proposed MPPT algorithm is shown in Fig. 3.

4.1 Analysis and design of reference signal for the proposed control

Reference [32] indicates that in power ranges under 200 Watts DCM control strategy achieves higher efficiency over boundary conduction mode (BCM). Moreover, DCM is easier than CCM in the case of control strategy since it does not have a right half plane zero and can have higher loop crossover frequency allowing wider transient response bandwidth. Thus, in this paper the DCM is considered.

The MPPT plus constant *v/f* control block is responsible for determining the modulating signal in order to generate switching signals of unfolding bridge and main power switches.

As described, the MPPT block determines the amplitude of M_{ref}. Here, to maintain the maximum constant torque producing capability of the motor, the goal of water pumping systems, the constant *v/f* control strategy is used. The frequency and magnitude of the voltage applied to the stator of the motor must be a constant ratio in order to achieve constant *v/f* control. It guarantees that throughout the operating range, the amplitude of the magnetic field in the stator is kept at an approximately constant level. The rated values of the frequency and magnitude of the stator voltage determine the *v/f* ratio. It should be noted that the voltage drop across the stator resistance must be compensated when the frequency and hence the voltage are low to keep the *v/f* ratio constant. Moreover, in order to avoid insulation breakdown at frequencies higher than the rated value, the constant *v/f* principle have to be violated [37]. It means that the stator voltage must not exceed the safety margin over its rated value. The scheme is shown in Fig. 4.

It is noticed that the output power P_{out} *(t)* during a half line period is a pulsating power following a squared sine wave given by:

$$P_{out}(t) = 2P_0 sin^2(\omega t) \tag{16}$$

where P_0 is the average output power.

Using M_{ref} and $Freq.^*$, the modulating signal is adjusted as:

$$Modulating\ Signal = M_{ref}|sin(2\pi \times F^*_{req.} \times t)| \tag{17}$$

where $Freq.^*$ is the reference frequency determined via the constant *V/f* control algorithm.

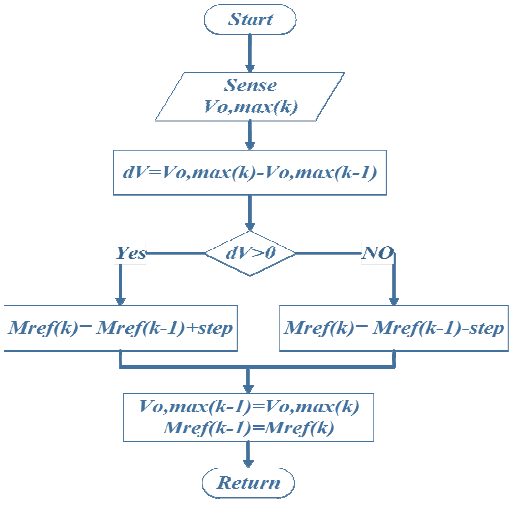

Fig. 3 *The proposed MPPT algorithm*

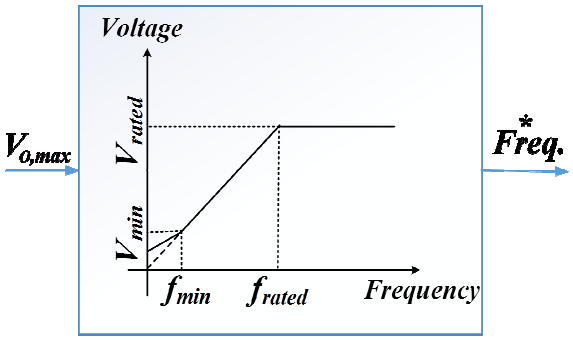

Fig. 4 *Voltage versus frequency under the constant V/f principle*

5. SIMULATION RESULTS

In order to analyze the proposed PV powered water pump system, a simulation platform based on PSIM 9.0 integrated with MATLAB is established. Table 1 presents the specifications of the simulation platform.

Table 1 Simulation Specifications

Parameter	***Symbol***	***Value***	***Unit***
Motor Specifications			
Rated Frequency	f_{rated}	50	Hz
Rated Voltage	V_{rated}	110	Vrms
Poles	P	2	
Stator Resistence	R_s	1.08	Ω
Stator Inductance	L_{ls}	6.8	mH
Rotor Resistance refered to the primary	R'_r	3.85	Ω
Rotor Inductance refered to the primary	L'_r	5.4	mH
Inverter Specifications			
Switching frequency	f_s	40	kHz
Transformer turn ratio	Np / Ns	1/12	
Input capacitance	C_{in}	11	mF
Output filter capacitance	C_f	1.64	μF
Output filter inductance	L_f	1	mH
Magnitizing inductance	L_m	4	μH
Leakage inductance	L_l	0.1	μH
PV Panel Specifications			
PV module maximum power	P_{max}	185	W
PV module voltage at P_{max}	V_{mpp}	23.5	V
PV module current at P_{max}	I_{mpp}	7.87	A

Fig. 5 shows the key waveforms under full load condition. Fig. 5 (a) shows that the envelope of primary current matches the reference signal. Fig. 5 (b) illustrates the details of the primary and secondary currents of the flyback inverter that verifies working under DCM. Fig. 5 (c) shows the current drawn by the motor.

Fig. 6 shows the output power of the PV panel and the control reference signal M_{ref} under step changes in irradiance in order to verify the performance of the proposed MPPT method. The system is working under full load condition, i.e. irradiance and temperature are 1000 W/m^2 and 25 $^{\circ}C$ respectively. At time *t=0.8,* a 250 W/m^2 step decrease in irradiance is occurred. At time *t=1.5,* irradiance is decreased to 500 W/m^2 (i.e. 50 percent of full load). At time *t=2.2,* a 250 W/m^2 step increase occurs. At time *t=2.9,* irradiance is increased to 1000 W/m^2. The MPPT algorithm has achieved the MPP under all indicated environmental conditions precisely.

Voltage stress across the main switches S_{m1} & S_{m2} is shown in Fig. 7. As the inverter is working at MPP, the input voltage is 23.5 volts. From Fig. 7, it is noted that the maximum voltage stress across main switches is limited to the input voltage as expected.

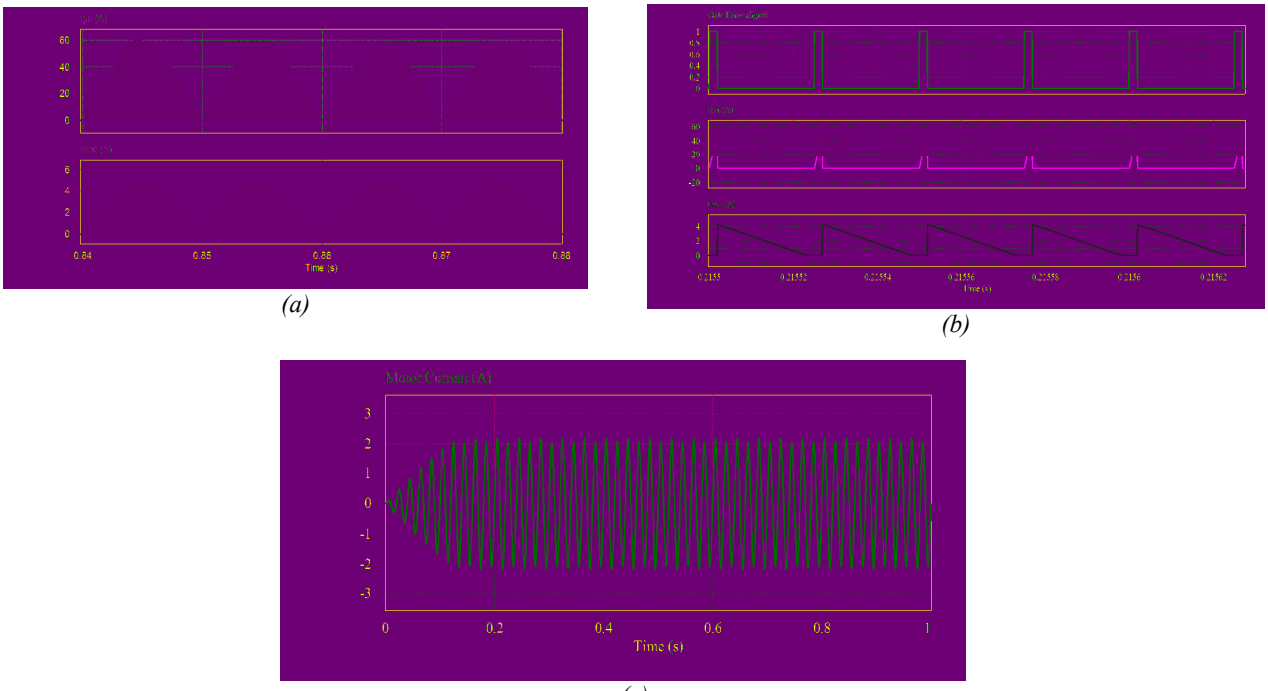

(a) *(b)* *(c)*

Fig. 5 *Key waveforms (a) Primary and Secondary currents. (b) Primary and Secondary currents, expanded waveforms. (c) Current drawn by the load.*

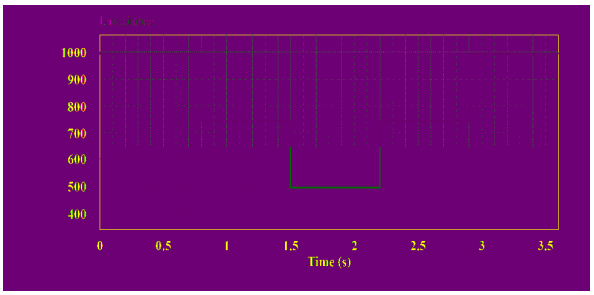

(a)

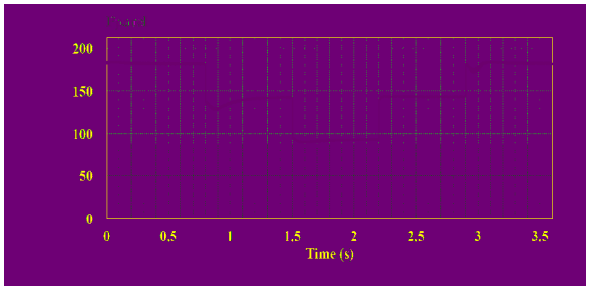

(b)

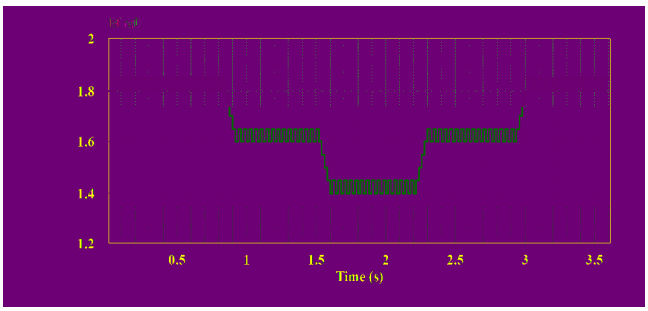

(c)

Fig. *6 Dynamic performance of the proposed system*
(a) Applied irradiance. (b)PV output power.
(c)Control signal.

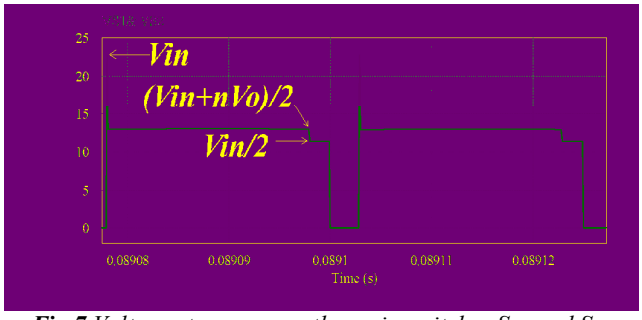

Fig.*7 Voltage stress across the main switches* S_{m1} *and* S_{m2}

6. EXPERIMENTAL RESULTS

To verify the proposed control system, a 200 W prototype of the proposed two-switch flyback inverter has been built. The specifications are the same as those in simulation section. A YL185-P23 YINGLI PV panel is used to verify the correctness of the proposed control method. Table 2 presents the specifications of the PV panel. Filter components values are the same as the simulation section.

The photo of the prototype is illustrated in Fig. 8. For experimental flexibility and ease of programming, a Texas Instruments TMS320f2812 DSP-based eZdsp kit is used for control and data acquisition. It should be noted that in a commercial product, a lower cost microcontroller would be more than adequate to implement the proposed control algorithm.

Fig.9 shows the primary and secondary currents which match the simulation results in Fig. 5. The currents are measured via a PINTEK ePA-677 current probe with 50 millivolt per ampere attenuation factor.

The voltage stress across main switches S_{m1} and S_{m2} is shown in Fig. 10. The voltage is measured with 10x attenuation. As described in the simulation section, the maximum voltage stress is limited to the input voltage which is the merit of the two-switch flyback topology.

The supplying current waveform before and after filtering and the output voltage waveform are shown in Fig. 11. The amplitude of the voltage fluctuates due to the operation of the MPPT algorithm that verifies the dynamic operation of MPPT algorithm. The voltage is measured with 10x attenuation.

To verify the dynamic performance of the proposed system, positive and negative step changes in irradiance are performed. As shown in Fig. 12, at time t_0, half of the PV panel surface is covered by a non-transparent object in order to simulate a step decrease in irradiance. Subsequent to this, at time t_1, the object is removed, causing the irradiance return to its previous level. Fig. 12 (a) shows the output voltage under this scenario. The voltage is measured with 10x attenuation. Prior to time t_0, the output voltage amplitude is about 150 volts, and the frequency is 50 Hz, the rated values at full load condition (Fig. 12 (b)). Subsequent to time t_0, as the amplitude of irradiance decreases, the voltage magnitude decreases to about 75 volts, and frequency halves which keeps *v/f* ratio constant (Fig. 12 (c)). When the irradiance returns to its value at full load condition at time t_1, the output voltage starts rising up to 150 volts, and frequency increases to 50 Hz both of which are the rated values at full load condition.

Table 2 PV panel Specifications

PV Panel Specifications			
PV module maximum power	P_{max}	185	W
PV module voltage at P_{max}	V_{mpp}	23.5	V
PV module current at P_{max}	I_{mpp}	7.87	A
Open circuit voltage	V_{oc}	29.5	V
Short circuit current	$I_{s.c.}$	8.45	A

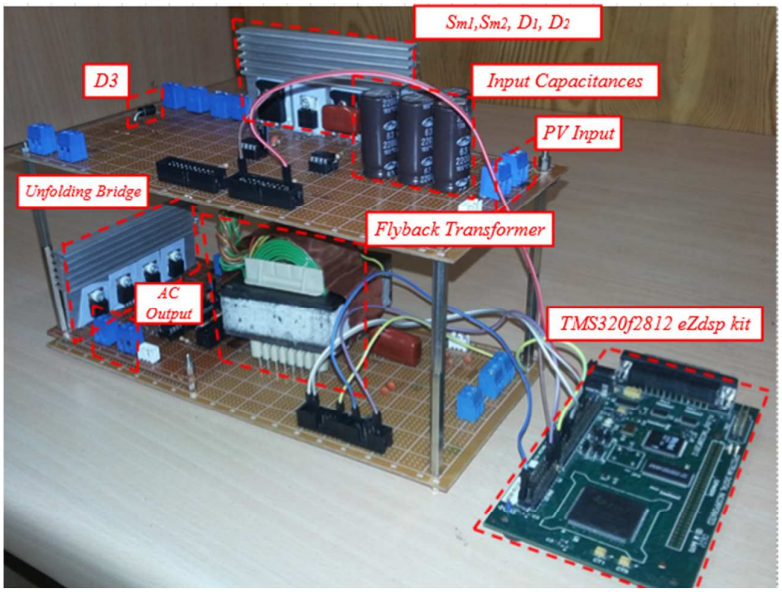

Fig. 8 *Photo of the prototype*

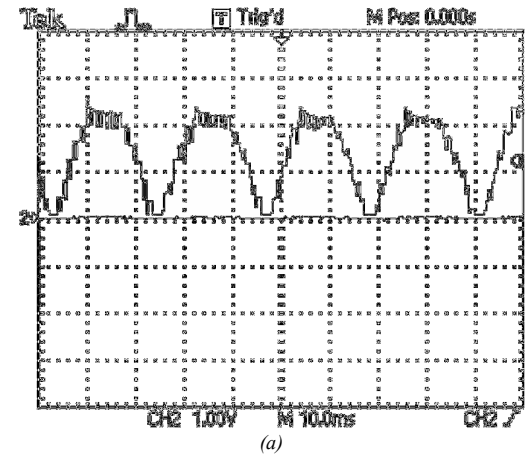

(a)

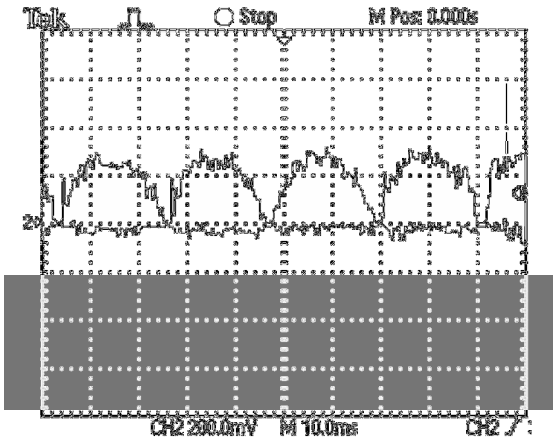

(b)

Fig. 9 *(a) Primary current. (b) Secondary current (experimental results)*

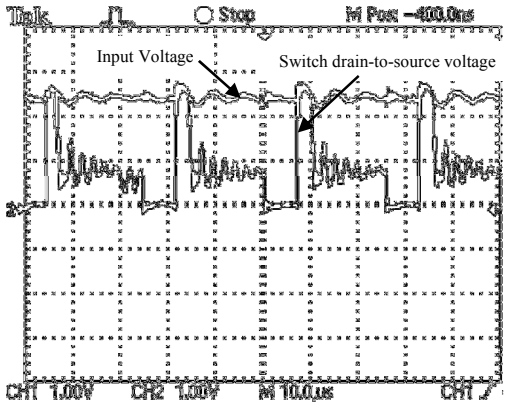

Fig. 10 *Switch drain-to-source voltage waveform and the input voltage (experimental results)*

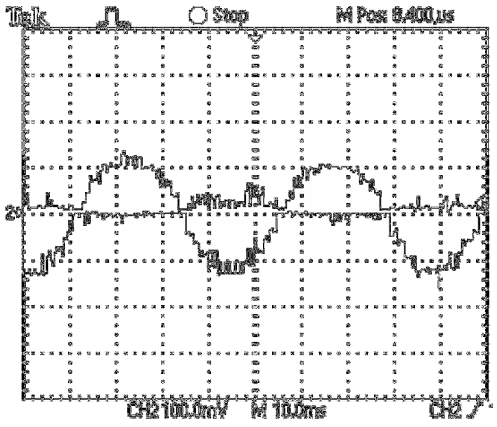

(a)

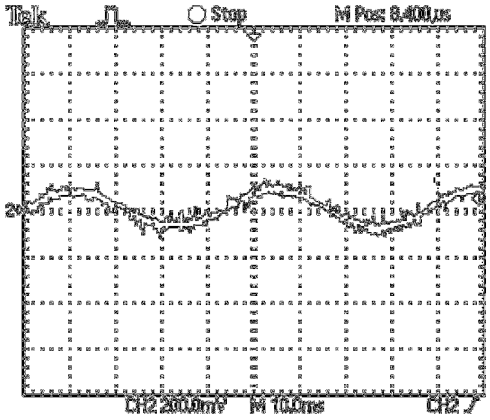

(b)

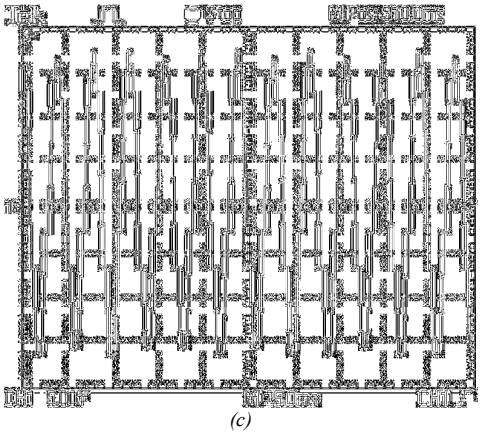

(c)

Fig. 11 *The supplying current and voltage waveforms*
(a) Current before filtering
(b) Current after filtering
(c) Supplying voltage waveform (experimental results)

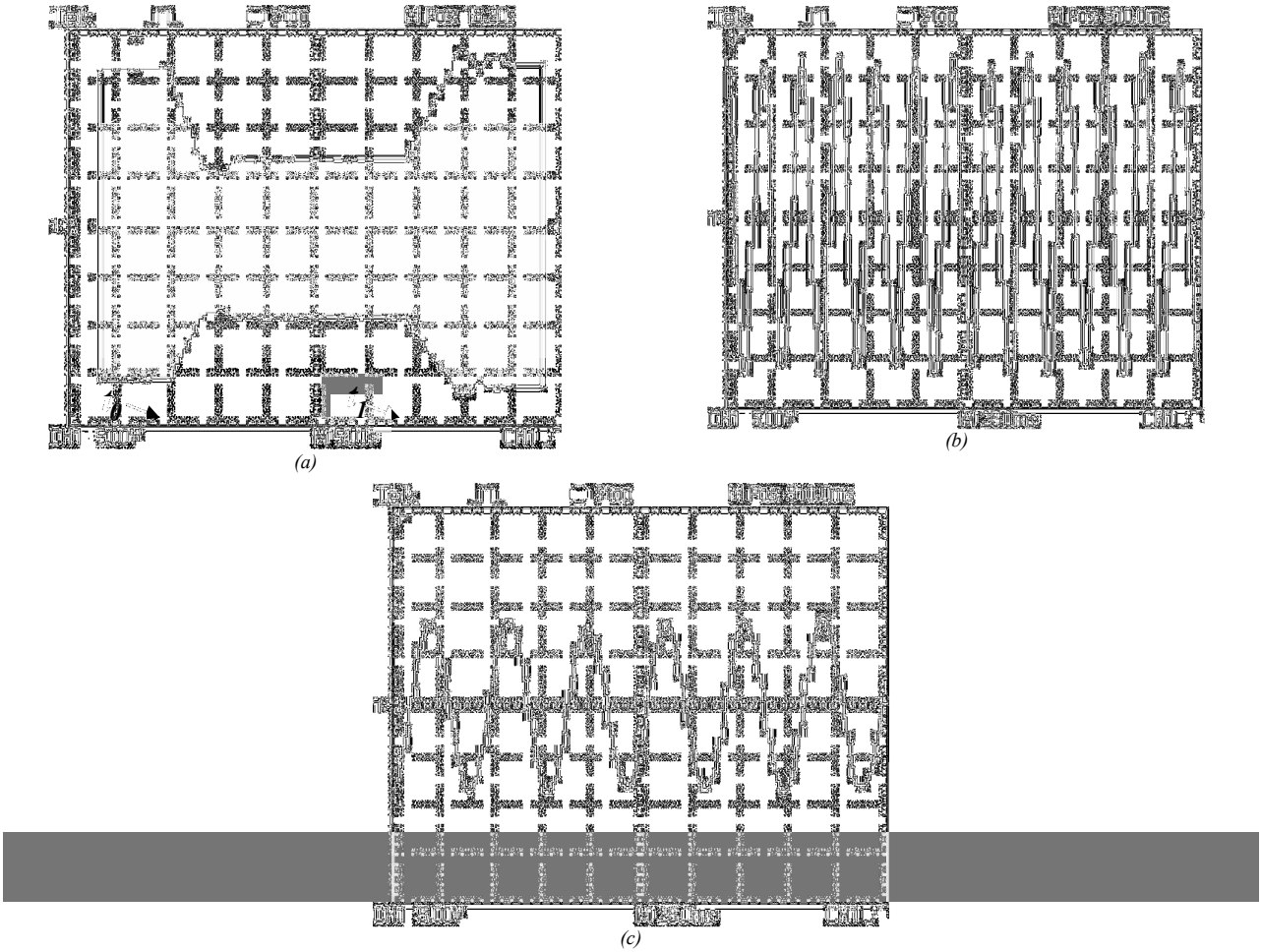

(a) *(b)* *(c)*

Fig. 12 *(a) Supplying voltage waveform under step changes in irradiance. (b) Expanded supplying voltage waveform at full load. (c) Expanded supplying voltage waveform at half load. (experimental results)*

7. CONCLUSION

In this paper, an off-grid two-switch flyback inverter using a current sensorless MPPT algorithm for fractional horse power water pumping systems was presented. The proposed inverter topology mitigates the problems of the conventional flyback inverter. The proposed MPPT method requires only the amplitude of the output voltage which both simplifies the implementation and also minimizes the cost. To verify the performance of the proposed inverter topology and the proposed control algorithm, simulation and experimental results were presented.

8. References

[1] Vitorino, M. A., de Rossiter Correa, M. B., Jacobina, C. B.: 'An effective induction motor control for photovoltaic pumping', *IEEE Trans. Ind. Electron.*, 2011, **58**, (4), pp. 1162–1170

[2] Alghuwainem, S. M.: 'Steady-state performance of DC motors supplied from photovoltaic generators with step-up converter', *IEEE Trans. Energy Convers.*, 1992, **7**, (2), pp. 267–272

[3] Pimkumwong, N., Onkrong, A., Sapaklom, T.: 'Modeling and simulation of direct torque control induction motor drives via constant volt/hertz technique', Elsevier Int. Conf. Advances in Computional modeling and simulation, 2012, **31**, pp. 1211–1216

[4] Henrique dos Santos, T., Goedtel, A., Oliveira da Silva, S.A., *et al.*: 'Scalar control of an induction motor using a neural sensorless technique', *Elsevier Electeric Power Syst. Research,* 2014, **108**, pp. 322–330

[5] Esram, T., Chapman, P. L.: 'Comparison of photovoltaic array maximum power point tracking techniques', *IEEE Trans. Energy Convers.,* 2007, **22**, (2), pp. 439–449

[6] Rezk, H., Eltamaly, A. M.: 'A comprehensive comparison of different MPPT techniques for photovoltaic systems', *Elsevier Solar Energy,* 2015, **112**, pp. 1–11

[7] Jain, S., Agarwal, V.: 'A new algorithm for rapid tracking of approximate maximum power point in photovoltaic systems', *IEEE Power Electron. Lett.*, 2004, **2**, (1), pp. 16–19

[8] Tey, K. S., Mekhilef, S.: 'Modified incremental conductane MPPT algorithm to mitigate inaccurate response under fast-charging solar irradiation level', *Elsevier Solar Energy,* 2014, **101**, (1), pp. 333–342

[9] Gao, L., Dougal, R. A., Liu, S., *et al.*: 'Parallel-Connected solar PV system to address partial and rapidly fluctuating shadow conditions', *IEEE Trans. Ind. Electron.,* 2009, **56**, (5), pp. 1548–1556

[10] Piegari, L., Rizzo, R.: 'Adaptive perturb and observe algorithm for photovoltaic maximum power point tracking', *IET Renew. Power Gener.,* 2010, **4**, (4), pp. 317–328

[11] Zakzouk, N. E., Elsaharty, M. A., Abdelsalam, A. K., *et al.*: 'Improved performancce low-cost incremental conductance PV MPPT technique', *IET Renew. Power Gener.,* 2016, **10**, (4), pp. 561–574

[12] Scarpa, V. V. R., Spiazzi, G., Buso, S.: 'Low complexity MPPT technique expliting the effect of the PV cell series resistance', Applied Power Electron. Conf. and Exposition (APEC), *May* 2008, pp. 1958–1964

[13] Sokolov, M., Shmilovitz, D.: 'A modified MPPT scheme for accelerated convergence', *IEEE Trans. Energy Convers.,* 2009, **23**, (4), pp. 1105–1107

[14] Leppaaho, J., Suntio, T.: 'Dynamic properties of PCM-controlled current-fed boost converter in photovoltaic system interfacing', Proc. 14th European Conf. Power Electronics Applications (EPE), 2011, pp. 1–10

[15] Fathabadi, H.: 'Novel fast dynamic MPPT (maximum power point tracking) technique with the capability of very high accurate power tracking', *Elsevier Energy,* 2016, **94**, pp. 466–475

[16] Sera, D., Teodorsecu, R., Hantschel, G., *et al.*: 'Optimized maximum power point tracker for fast-changing environmental conditions', *IEEE Trans. Ind. Electron.,* 2008, **55**, (7), pp. 2629–2637

[17] Karbakhsh, F., Abootorabi Zarchi, H.: 'A fast and robust maximum power point tracker for photovoltaic systems using variable structure control approach', 23rd Iranian Conf. Electrical Eng. (ICEE), 2015, pp. 1647-1652

[18] Meza, C., Biel, D., Negroni, J., *et al.*: 'Boost-buck inverter variable structure control for grid-connected photovoltaic systems with sensorless MPPT', Proc. IEEE Int. Symp. on Industrial Electronics, 2005, **2**, pp. 657–662

[19] Rahim, N. A., Selvaraj, J., Krismadinata, C.: 'Hysteresis current control and sensorless MPPT for grid-connected photovoltaic systems', IEEE Int. Symp. on Industrial Electronics, 2007, pp. 572–577

[20] Yang, B., Li, W., Zhao, Y., *et al.*: 'Design and analysis of a gridconnected photovoltaic power system', *IEEE Trans. Power Electron.,* 2010, **25**, (4), pp. 992–1000

[21] Kim, Y., Kang, J., Youn, S., *et al.*: 'Sensorless current balancing and MPPT control for photovoltaic AC module type interleaved flyback inverter', 7th Int. Power Electronics and Motion Control Conf. (IPEMC), 2012, pp. 1363–1367

[22] Kitano, T., Matsui, M., De-hong Xu.: 'Power sensor-less MPPT control scheme utilizing power balance at DC linksystem design to ensure stability and response', IEEE Conf. Industrial Electronics Society, 2001, **2**, pp. 1309–1314

[23] Park, S., Jinda, A. K., Gole, A. M., *et al.*: 'An optimized sensorless MPPT method for PV generation system', Canadian Conf. Electrical and Computer Eng. (CCECE), 2009, pp. 720–724

[24] Jain, S., Agarwal, V.: 'Comparison of the performance of maximum power point tracking schemes applied to single-stage grid-connected photovoltaic systems', *IET Electric Power Applications*, 2007, **1**, (5), pp. 753–762

[25] Patel, H., Agarwal, V.: 'MPPT scheme for a PV-fed single-phase single-stage grid-connected inverter operating in CCM with only one current sensor', *IEEE Trans. Energy Convers.*, 2009, **24**, (1), pp. 256–263

[26] Kutkut, N., Hu, H.: 'Photovoltaic micro-inverter: topologies, control aspects, reliability issues, and applicable standards', Proc. IEEE Energy Conversion Congress and Exposition (ECCE), 2010, tutorial

[27] Martins, D. C., Demonti, R.: 'Grid connected PV system using two energy processing stages', 29th IEEE Photovoltaic Specialists Conf., 2002, pp. 1649–1652

[28] Shimzu, T., Wada, K., Nakamura, N.: 'Flyback type single-phase utility interactive inverter with power pulsation decoupling on the DC input for an AC photovoltaic module system', *IEEE Trans. Power Electron.*, 2006, **21**, (5), pp. 1264-1272

[29] Kyritsis, A. Ch., Tatakis, E. C., Papanikolaou, N. P.: 'Optimum design of the current-source flyback inverter for decentralized grid- connected photovoltaic systems', *IEEE Trans. Energy Convers.*, 2008, **23**, (1), pp. 281-293

[30] Nanakos, A. C., Tatakis, E. C., Papanikolaou, N. P.: 'A weighted-efficiency-oriented design methodology of flyback inverter for AC photovoltaic modules', *IEEE Trans. Power Electron.*, 2012, **27**, (7), pp. 3221-3233

[31] Li, Y., Oruganti, R.: 'A low cost flyback CCM inverter for AC module application', *IEEE Trans. Power Electron.*, 2012, **27**, (3), pp. 1295-1303

[32] Zhang, Z., He, X., Liu, Y.: 'An optimal control method for photovoltaic grid-tied interleaved flyback micro-inverters to achieve high efficiency in wide load range', *IEEE Trans. Power Electron.*, 2013, **28**, (11), pp. 5074-5087

[33] Kjaer, S. B., Blaabjerg, F.: 'Design optimization of a single phase inverter for photovoltaic applications', IEEE 34th Annu. Power Electronics Specialist Conf., 2003, **3**, pp. 1183–1190

[34] Kazimierczuk, K. M.: 'Pulse-width Modulated DC-DC Power Converters' (John Wiely and Sons,2008), pp. 189-236.

[35] Ali, A. N. A., Saied, M. H., Mostafa, M. Z., *et al.*: 'A survey of maximum PPT techniques of PV systems', IEEE Energytech Conf., 2012, pp. 1–17

[36] Shmilovitz, D.: 'On the control of photovoltaic maximum power point tracker via output parameters', *Proc. IEE Electric Power Applications,* 2005, **152**, (2), pp. 239–248

[37] Yu, Z., Figoli, D.: 'AC induction motor control using constant V/Hz principle and space vector PWM technique with TMS320C240', (TI application report, 1998)

[38] Gao, M., Chen, M., Zhang, C., *et al.*: 'Analysis and implementation of an improved flyback-inverter for photovoltaic AC module applications', *IEEE Trans. Power Electron.*, 2014, **29**, (7), pp. 3428-3444